Sensor Diaphragm Under Initial Tension: Linear Analysis

by M. Yu and B. Balachandran

ABSTRACT—In this paper, we present recent efforts conducted to investigate the dynamic behavior of a sensor diaphragm under initial tension. A comprehensive mechanics model based on a plate with in-plane tension is presented and analyzed to examine the transition from plate behavior to membrane behavior. It is shown that for certain tension parameter values, it is appropriate to model the diaphragm as a plate–membrane structure rather than as a membrane. The model predictions are found to compare well with experimental results. The analysis and results should be valuable for carrying out the design of circular sensor diaphragms for various applications.

KEY WORDS—Diaphragm, pressure sensor, plate with in-plane tension, linear analysis

Introduction

A common element of different pressure sensors, which include silicon piezoresistive sensors, capacitive sensors, and fiber-optic sensors, is a diaphragm structure.[1–4] The vibration of this diaphragm structure is detected either through the displacement of the diaphragm or through the strain induced in the diaphragm by the vibration. In recent work,[3–6] both of these means have been considered for designing appropriate mechanical elements for fiber-optic pressure sensors. The sensor sensitivity, bandwidth, and linearity are directly related to the structural behavior of the diaphragm. In a typical condenser microphone, the diaphragm is a stretched thin structure, for which membrane equations are usually used for analyzing the diaphragm vibrations.[7] Static membrane equations have also been used in other sensor designs.[1–4] However, a membrane model is not always the most appropriate one.

Sheplak and Dugundji[8] carried out static analysis of a clamped circular plate under initial tension and studied the transition range from plate behavior to membrane behavior in terms of the tension parameter k. For "small" plate deflections, they have shown that the transition from plate behavior to membrane behavior can be described in terms of the nondimensional tension parameter k. This transition occurs over the range $1 < k < 20$, with the plate behavior dominating for $k < 1$ and the membrane behavior dominating for $k > 20$.

M. Yu is an Assistant Professor and B. Balachandran (balab@glue.umd.edu) is a Professor, Department of Mechanical Engineering, University of Maryland, College Park, Maryland 20742, USA.

Original manuscript submitted: November 22, 2003.
Final manuscript received: December 21, 2004.
DOI: 10.1177/0014485105052319

Here, since the sensors of interest are meant for sound-pressure measurements, a dynamic analysis of the diaphragm is necessary to determine whether characteristics such as mode shapes and natural frequencies need to be determined from a plate model, a membrane model, or a plate–membrane model. To this end, the earlier work[8] is extended here to the dynamic case and the diaphragm response is characterized in terms of the tension parameter k. This analysis, which has not been carried out previously in the literature, is an important contribution to this effort. Furthermore, it is illustrated as to how this analysis and related results can be used to tailor the sensor diaphragm characteristics to achieve a high sensitivity and a high bandwidth. The rest of this paper is organized as follows. In the next section, the model of a plate with in-plane tension is provided and linear analysis is used to examine free oscillations. Subsequently, plate–membrane transition behavior is discussed and results obtained from a representative case (a Mylar diaphragm) are presented. In the fourth section, forced oscillations are considered and different results that can guide the design of a pressure-sensor diaphragm are presented. Comparisons with experimental results are also included in this section. Concluding remarks are provided in the final section.

Model Description and Free Oscillations

Figure 1 illustrates a clamped, circular diaphragm of radius of a and thickness h. The Young's modulus of elasticity and Poisson's ratio of the diaphragm material are denoted by E and v, respectively. The initial tension per unit length applied to the diaphragm is represented by N_0.

A nondimensional tension parameter k is defined as

$$k = a\sqrt{\frac{N_0}{D}} = \frac{a}{h}\sqrt{\frac{12(1-v^2)N_0/h}{E}} = \frac{a}{h}\sqrt{\frac{12(1-v^2)T}{E}} \tag{1}$$

where the constant $D = Eh^3/(12(1\text{-}v^2))$ and $T = N_0/h$ is the tension per unit area. In the analysis that follows, it is shown that the choice of a plate model or a membrane model actually depends on the tension parameter k, not on just the initial tension per unit length N_0 applied to the diaphragm.

Linear Model of Plate with Tension

Starting from Love's equations,[9] including damping, axial in-plane force per unit length N_r, and the transverse loading per unit area $f(r, \theta; t)$, the nonlinear partial differential

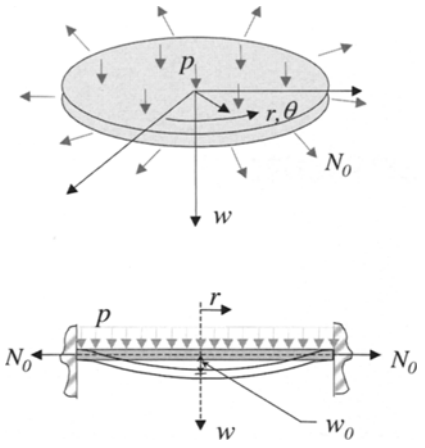

Fig. 1—Illustration of a diaphragm clamped along its edge

equation governing a plate with initial tension can be obtained as

$$\rho h\frac{\partial^2 w}{\partial t^2} + D\nabla^4 w - N_0\nabla^2 w = \frac{1}{r}\frac{\partial}{\partial r}\left(rN_r\frac{\partial w}{\partial r}\right) - 2\mu\frac{\partial w}{\partial t} + f(r,\theta;t) \quad (2)$$

where r is the radial distance from the center, θ is the angular coordinate, $w(r, \theta; t)$ is the transverse displacement, and μ is the damping coefficient. For "small" displacements, eq (2) can be reduced to the linear form[6]

$$\rho h\frac{\partial^2 w}{\partial t^2} + D\nabla^4 w - N_0\nabla^2 w = -2\mu\frac{\partial w}{\partial t} + f(r,\theta;t). \quad (3)$$

The boundary conditions along the clamped edge at $r = a$ and the requirement that the displacement be finite at the plate center (i.e., $r = 0$) are given by

$$\begin{aligned} &w(r,\theta;t)|_{r=a} = 0,\ \left.\frac{\partial w(r,\theta;t)}{\partial r}\right|_{r=a} = 0 \\ &|\,w(r,\theta;t)|_{r=0}\,| < \infty. \end{aligned} \quad (4)$$

Free Oscillations of Undamped System

In the absence of damping and forcing, a solution of the form

$$w(r,\theta,t) = W(r,\theta)\cos\omega t \quad (5)$$

is assumed, where ω is the natural frequency. After substituting eq (5) into eq (3), the result is

$$-\rho h\omega^2 W + D\nabla^4 W - N_0\nabla^2 W = 0. \quad (6)$$

Noting that eq (6) can be written as

$$\left(\nabla^2 - \alpha_1^2\right)\left(\nabla^2 + \alpha_2^2\right)W = 0, \quad (7)$$

it is found that

$$\begin{aligned} \alpha_1^2 &= \frac{N_0 + \sqrt{N_0^2 + 4\rho h\omega^2 D}}{2D} \\ \alpha_2^2 &= \frac{-N_0 + \sqrt{N_0^2 + 4\rho h\omega^2 D}}{2D}. \end{aligned} \quad (8)$$

Next, expanding the transverse displacement amplitude as

$$W(r,\theta) = R(r)\Theta(\theta) \quad (9)$$

and substituting into the spatial eigenvalue problem given by eq (7), it is determined that

$$\begin{aligned} \Theta(\theta) &= A_m\cos m(\theta - \varphi_m) \\ R(r) &= A_{1m}I_m(\alpha_1 r) + A_{2m}K_m(\alpha_1 r) \\ &\quad + A_{3m}J_m(\alpha_2 r) + A_{4m}Y_m(\alpha_2 r) \end{aligned} \quad (10)$$

where m is an integer since the plate is closed in the θ direction, and A_m, φ_m, and A_{im} are constants to be determined. The functions $I_m(\alpha_1 r)$, $K_m(\alpha_1 r)$, $J_m(\alpha_2 r)$, and $Y_m(\alpha_2 r)$ are the modified Bessel function of the first kind, the modified Bessel function of the second kind, the Bessel function of the first kind, and the Bessel function of the second kind, respectively. Each of these functions is of order m.

From eqs (4), (5), (9), and (10), the finite displacement condition at the plate center leads to

$$A_{2m} = A_{4m} = 0. \quad (11)$$

Making use of the clamped edge boundary conditions given by eq (4) in eqs (5), (9), and (10), the characteristic equation is determined to be

$$I_m(\alpha_{1m}a)J'_m(\alpha_{2m}a) - J_m(\alpha_{2m}a)I'_m(\alpha_{1m}a) = 0, \quad (12)$$

where the prime indicates a derivative with respect to r. Determining the roots of eq (12) for each value of m and labeling them successively using the integer index n, it is found that the natural frequencies are given by

$$\omega_{mn}^2 = \frac{D}{\rho h a^4}(\alpha_{2mn}a)^2\left[(\alpha_{2mn}a)^2 + k^2\right] \quad (13)$$

where k is the tension parameter introduced in eq (1). The associated mode shapes are given by

$$W_{mn}(r,\theta) = A_{mn}\left[J_m(\alpha_{2mn}r) - \frac{J_m(\alpha_{2mn}a)}{I_m(\alpha_{1mn}a)}I_m(\alpha_{1mn}r)\right]\cos m(\theta - \varphi_m). \quad (14)$$

Plate–membrane Transition Behavior and Results

Here, the results of the previous section are used to examine the free-oscillation characteristics in the limiting cases of plate behavior and membrane behavior and the transition cases between them.

Membrane Model (D=0)

First, it follows that as $D \to 0$, $\frac{D}{N_0} \to 0$ and from eq (1) that $k \to \infty$. Then, from eqs (8), (13), and (14), noting that $\alpha_1 \to \infty$, it is found that the associated natural frequencies and the mode shapes are given by

$$\begin{aligned} \omega_{mn} &= \alpha_{2mn}\sqrt{\frac{N_0}{\rho h}} \\ W_{mn}(r,\theta) &= A_{mn}J_m(\alpha_{2mn}r)\cos m(\theta - \varphi_m). \end{aligned} \quad (15)$$

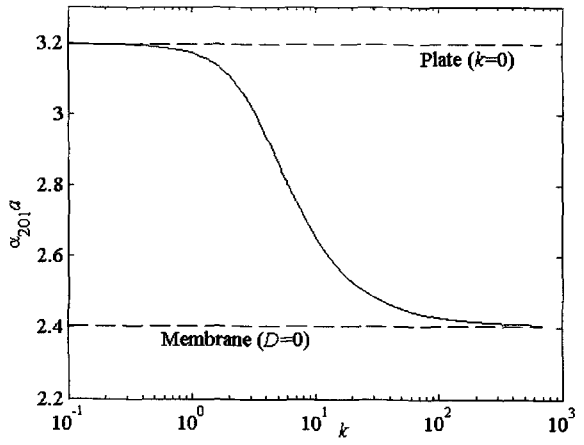

Fig. 2—First vibration mode: transition behavior with respect to the tension parameter k

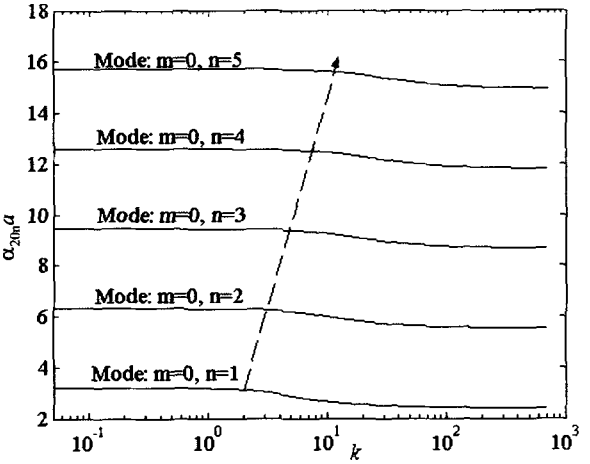

Fig. 3—Different vibration modes: transition behavior with respect to the tension parameter k

Plate Model ($N_0 = 0$)

For this case, from eq (1), it is noted that as $N_0 \to 0$, $k \to 0$, and from eqs (8), (13), and (14), noting that $\alpha_1 = \alpha_2$, it is found that the associated natural frequencies and the mode shapes are given by

$$\omega_{mn} = (\alpha_{2mn})^2 \sqrt{\frac{D}{\rho h}}$$

$$W_{mn}(r, \theta) = A_{mn}\left[J_m(\alpha_{2mn}r) - \frac{J_m(\alpha_{2mn}a)}{I_m(\alpha_{2mn}a)} I_m(\alpha_{2mn}r)\right] \cos m(\theta - \varphi_m). \tag{16}$$

Plate–membrane Transition

The results shown in Figs. 2–4 are applicable to any isotropic circular diaphragm whose edge is clamped. For the first vibration mode (i.e., $m = 0, n = 1$), the transition behavior from plate to membrane is shown in Fig. 2. To obtain this plot, the eigenvalue ($\alpha_{2mn}a$) is determined from eq (12) for different values of k. As k decreases and takes on values less than 2, the graph of ($\alpha_{2mn}a$) is asymptotic to the plate case (i.e., $\alpha_{2mn}a = 3.196$). As k increases and becomes larger than 20, the graph of ($\alpha_{2mn}a$) is asymptotic to the membrane case (i.e., $\alpha_{2mn}a = 2.404$). There is a transition from plate behavior to membrane behavior in the region of $2 < k < 20$. This result is similar to the obtained by Sheplak and Dugundji[8] for the static case. For higher vibration modes, this transition region also exists and it moves toward the direction of increasing k, as shown in Fig. 3.

In Fig. 4, the variations in the radial distributions $R_{mn}(r)$ of the first four mode shapes are shown with respect to the tension parameter k. As the order of the mode increases, the variation in the mode shape with respect to the tension parameter k is more pronounced.

Mylar Diaphragm: Natural Frequency Dependence on Different Parameters

As a representative case, we consider a Mylar diaphragm with a Young's modulus of elasticity E = 3.45 × 10^9 Pa, density $\rho = 1.29 \times 10^3$ kg m^{-3}, and Poisson's ratio $\upsilon = 0.41$. For a diaphragm radius of 1.75 mm and thickness of 40 μm, the dependence of each of the first four natural frequencies on the tension parameter k are shown in Fig. 5. As expected from eq (13), the natural frequencies are expected to increase as the tension parameter k is increased. When the tension parameter k is less than 2, the natural frequencies almost remain constant with respect to k. However, when k is larger than 20, the natural frequencies increase rapidly.

Figures 6 and 7 show, for $k = 0$, the variations in the first natural frequency with respect to the diaphragm radius and the diaphragm thickness. As expected, as either the radius is decreased or the thickness is increased, the first natural frequency of the diaphragm increases. Noting that a sensor's operating bandwidth is chosen to be less than the first natural frequency, the results of Figs. 5–7 are important for tailoring the diaphragm parameters in order to obtain the required sensor bandwidth.

To design a sound pressure sensor, it is desirable to have a small size. Here, the radius of a Mylar diaphragm is chosen to be a "small" constant value (e.g., a = 1.75 mm). In Fig. 8, the first natural frequency is plotted as a function of k for the diaphragm thicknesses of 5, 10, 20, 30, and 40 μm, respectively. From this figure, it is seen that it is possible to obtain the same natural frequency (10.7 kHz) as that for the diaphragm with h = 40 μm and k = 0 by choosing the tension parameters given in Table 1. Corresponding sensitivity curves for each h and k pair are shown in Yu.[5] It can be seen that for the diaphragm with the lower thickness, when the natural frequency is increased to 10.7 kHz by choosing an appropriate tension parameter, the resulting sensor has a higher sensitivity. It is also possible to achieve high sensitivity and high bandwidth simultaneously by increasing the diaphragm radius and applying an appropriate tension. However, a small sensor size is always more preferable when a high spatial resolution is required.

Forced Oscillations

To consider the forced response of a damped diaphragm to harmonic excitations, eq (3) is considered and the loading

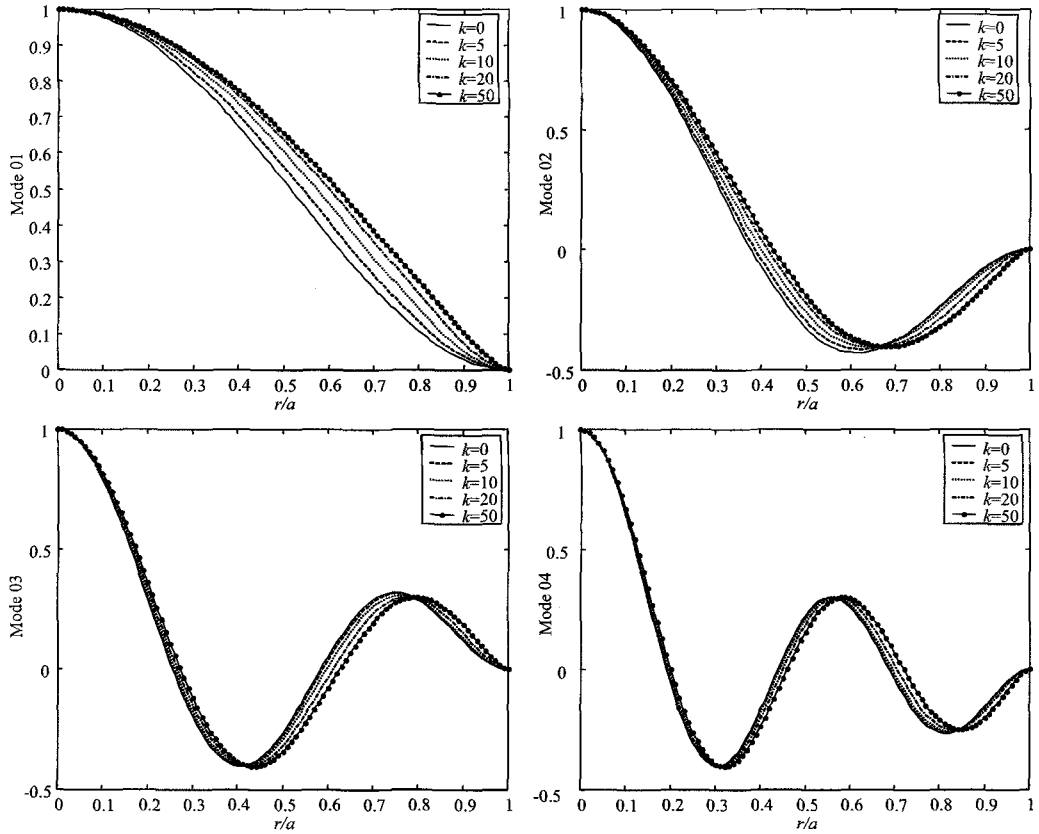

Fig. 4—Variations in the first four mode shapes with respect to the tension parameter k

TABLE 1—VALUES OF k, N_0, AND T FOR DIFFERENT h TO OBTAIN THE SAME NATURAL FREQUENCY AS A DIAPHRAGM WITH $h = 40$ μm AND $k = 0$

h (μm)	K	N_0 (N m^{-1})	T (N m^{-2})
5	32.86	14.8052	2.9610×10^6
10	15.73	3.3926	0.6785×10^6
20	6.86	0.6453	0.1291×10^6
30	3.45	0.1632	0.0326×10^6

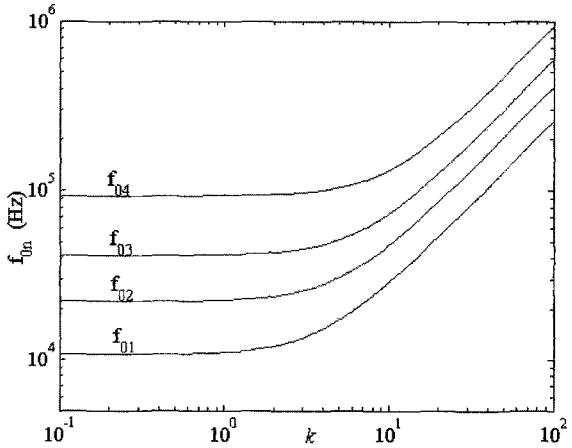

Fig. 5—Variations of the first four natural frequencies with respect to the tension parameter k

is assumed to be of the form

$$f(r, \theta; t) = p(r, \theta)e^{j\omega t} \tag{17}$$

where the pressure amplitude $p(r, \theta)$ is assumed to be uniform and denoted by p, and ω is the excitation frequency.

The interest is in primarily determining the steady-state response of the diaphragm, when it is excited close to the diaphragm's first natural frequency. To that end, a single-mode approximation is assumed as

$$w(r, \theta, t) \approx W_{01}(r, \theta)\eta_1(t) \tag{18}$$

where η_1 is the modal amplitude and W_{01} is the first mode shape of the undamped linear system discussed in the second and third sections. After making use of eqs (17) and (18) in eq (3), the approximation for the steady-state forced response of the diaphragm can be obtained as

$$w(r, \theta; t) \approx U(r, \theta)e^{j(\omega t - \varphi_0)} = \Lambda_{01} W_{01}(r, \theta)\, e^{j(\omega t - \varphi_0)} \tag{19}$$

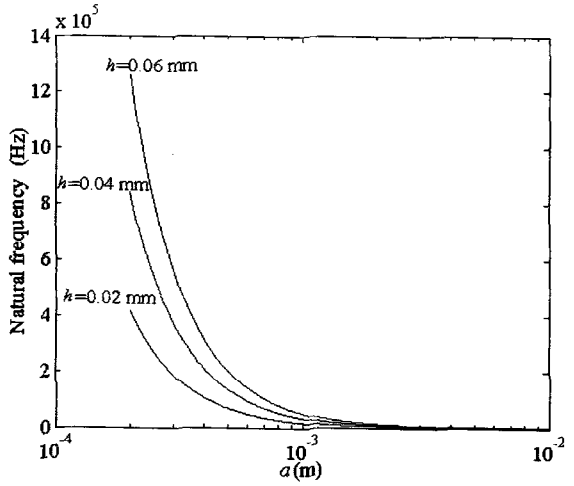

Fig. 6—Variation of the first natural frequency with respect to the diaphragm radius for different values of the diaphragm thickness

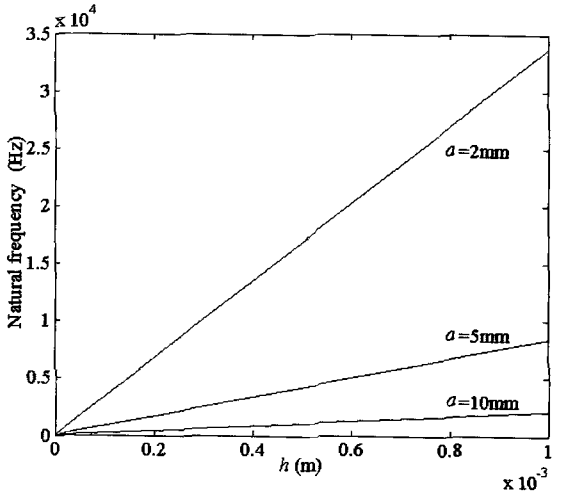

Fig. 7—Variation of the first natural frequency with respect to the diaphragm thickness for different diaphragm radii

where $U(r, \theta)$ is the displacement amplitude,

$$\Lambda_{01} = \frac{F_1}{\omega_1^2\sqrt{\left[1-\left(\frac{\omega}{\omega_1}\right)^2\right]^2+4\zeta_1^2\left(\frac{\omega}{\omega_1}\right)^2}}$$
$$W_{01}(r,\theta) = A_{01}\left[J_0(\alpha_{201}r) - \frac{J_0(\alpha_{201}a)}{I_0(\alpha_{101}a)} I_0(\alpha_{101}r)\right] \quad (20)$$

and A_{01} and φ_0 are appropriate constants. Further,

$$\zeta_1 = \frac{\mu}{\rho h \omega_1}, \quad F_1 = \frac{p}{\rho h N_1}\int_0^a W_{01}(r,\theta)2\pi r\, dr, \quad \text{and}$$

$$N_1 = \frac{1}{A_{01}^2}\int_0^a 2\pi r W_{01}^2(r,\theta)dr. \quad (21)$$

From eqs (20) and (21), the amplitude of diaphragm displacement at the center (i.e., $r = 0$) is found to be

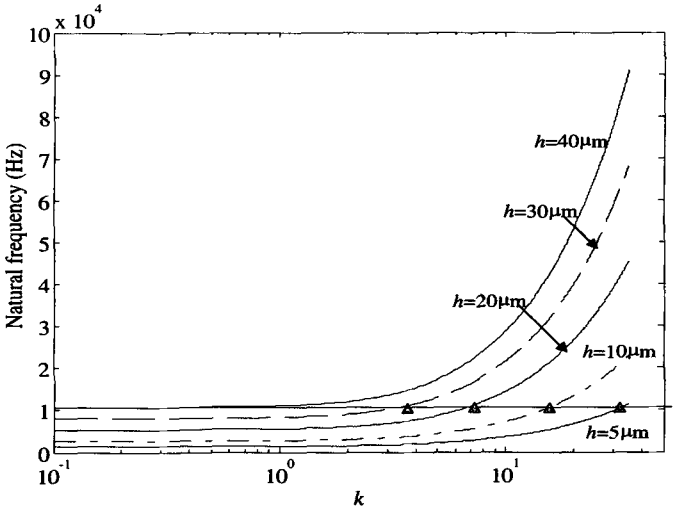

Fig. 8—Variation of first natural frequency with respect to k for different thicknesses

$$U_0(r=0,\theta) = \quad (22)$$
$$\frac{2\pi pa}{\rho h N_1}\cdot\frac{\left[\frac{1}{\alpha_{201}}J_1(\alpha_{201}a)-\frac{J_0(\alpha_{201}a)}{\alpha_{101}I_0(\alpha_{101}a)}I_1(\alpha_{101}a)\right]\left[1-\frac{J_0(\alpha_{201}a)}{I_0(\alpha_{101}a)}\right]}{\omega_1\sqrt{\left[1-\left(\frac{\omega}{\omega_1}\right)^2\right]^2+4\zeta_1^2\left(\frac{\omega}{\omega_1}\right)^2}}.$$

Equation (22) will be used to study the sensitivity of the diaphragm response to various parameters next.

Displacement Variation With Respect to Tension Parameter, Diaphragm Radius, and Diaphragm Thickness

Figure 9 shows the results for the case when a Mylar diaphragm of 1.75 mm radius and 40 μm thickness is subjected to a 10 kHz excitation and pressure amplitude of 1 Pa. In the undamped case (i.e., $\zeta_1 = 0$), there is plate-type behavior for $k < 1$. As the value of the tension parameter is increased, there is a transition region from a plate-type behavior to a membrane-type behavior. This is similar to what is seen in Figs. 2 and 3, where the natural frequencies are plotted with respect to the parameter k. With the inclusion of damping, in each damped case, the window of plate-type behavior is expanded while the transition region becomes smaller. For $k > 20$, there is a membrane-type behavior region with the displacement amplitude decreasing rapidly with increase in the tension.

As discussed in the third section, increasing the in-plane tension can increase the natural frequencies. However, this will result in a decrease of the displacement amplitude of diaphragm center. From a sensor design standpoint, increasing the tension can enhance the sensor bandwidth but it reduces the sensitivity. This becomes a trade-off issue between the sensitivity and the sensor bandwidth that one needs to address, when designing a diaphragm. For a constant value of tension k (here, $k = 0$), the displacement amplitude of a diaphragm center will increase when the thickness is decreased and/or the radius is increased, as shown in Fig. 10. However,

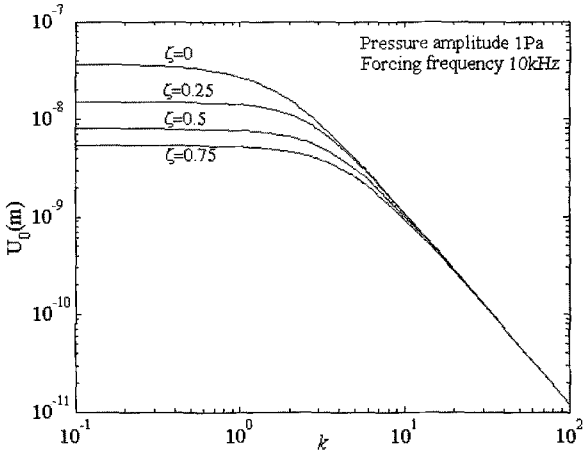

Fig. 9—Variation of the displacement amplitude at the diaphragm center with respect to tension parameter k for different damping factors

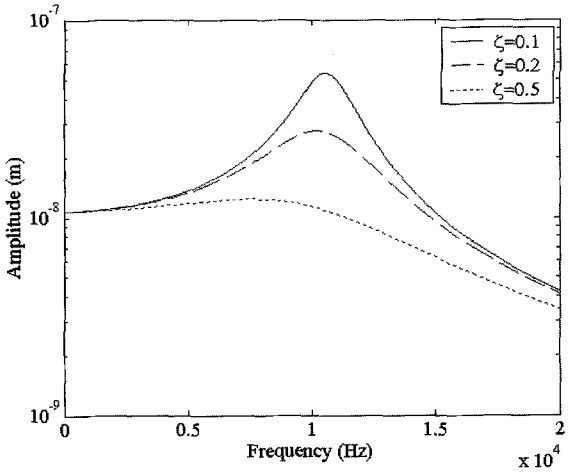

Fig. 11—Frequency–response curves for different damping factor values

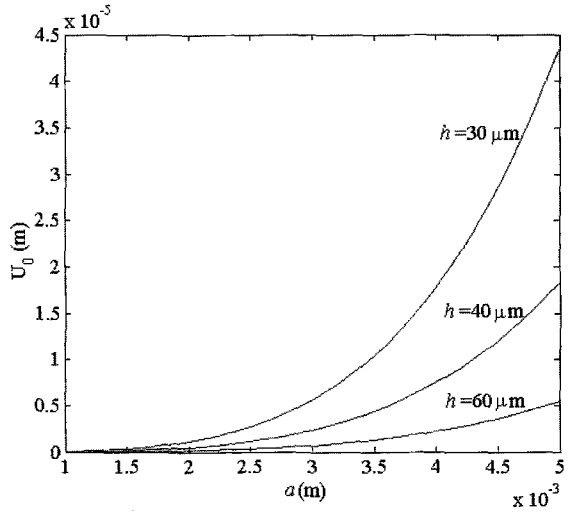

Fig. 10—Variation of the displacement amplitude at the diaphragm center with respect to the diaphragm radius for different thickness values

as discussed in the previous section, by doing this, the first natural frequency will decrease, resulting in a smaller sensor bandwidth. This turns out to be another trade-off issue between the sensor bandwidth and the sensitivity that one has to deal with, in designing a sensor.

Sensor Bandwidth and Damping

Apart from the system's first natural frequency, damping is another parameter that can be used to tailor the system bandwidth. To illustrate this point, in Fig. 11, again for the Mylar diaphragm discussed previously ($k = 0$), the frequency–response curves are graphed for different values of the damping factor. As expected, with sufficient damping, the response at the first resonance is reduced considerably and the region of "fairly flat" response is extended close to the first natural frequency of the system.

Comparisons with Experimental Results

Experiments were conducted to study the relationship between the diaphragm displacement and the applied dynamic pressure at different excitation frequencies; with respect to Table 1, the parameters of the diaphragm studied in the experiment are $h = 30$ μm and $k = 3.45$, which corresponds to an intermediate behavior between plate-type behavior and membrane-type behavior. A loud speaker was used to generate a pressure loading on the diaphragm surface and a laser vibrometer was used to measure the displacement at the diaphragm center. A linear relationship was observed from experimental data shown in Fig. 12, for a selected value of the excitation frequency. This relationship compares well with the model prediction given by eq (22).

From the experiments, it was determined that the damping factor for the considered diaphragm is 0.03. The frequency–response curve determined from the model (eq (22)) is compared with experimental data in Fig. 13. These experimental data were obtained by using a white noise pressure loading on the diaphragm. Good agreement is found between the experimental results and model predictions.

Concluding Remarks

To close this paper, it is noted that when a diaphragm is to be used as a part of a pressure sensor, a dynamic analysis of the diaphragm is necessary. To this end, a model based on a plate with in-plane tension has been considered and analyzed here. The presented analysis and results are more comprehensive and accurate than those previously presented in the literature for either plate or membrane cases. As illustrated by the results, the dynamic behavior of the diaphragm exhibits a transition from plate behavior to membrane behavior, when the tension parameter k is between 2 and 20 with the plate behavior dominating for $k < 2$ and the membrane behavior dominating for $k > 20$. The model predictions are found to compare well with the experimental results. From the analysis and results obtained, it is clear that a high sensor bandwidth can be achieved by increasing

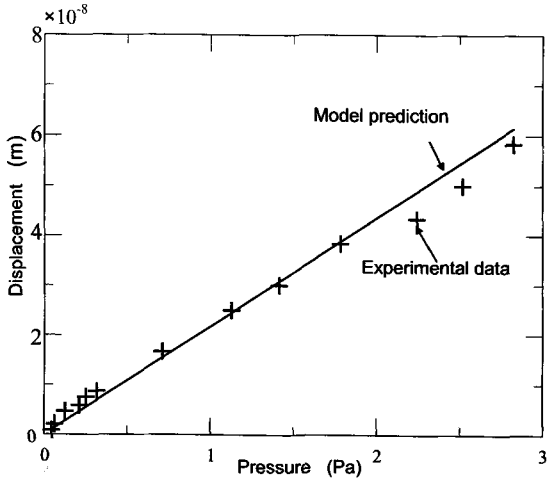

Fig. 12—Comparison of experimental results with model predictions for diaphragm displacement versus applied pressure. The excitation frequency is 1 kHz

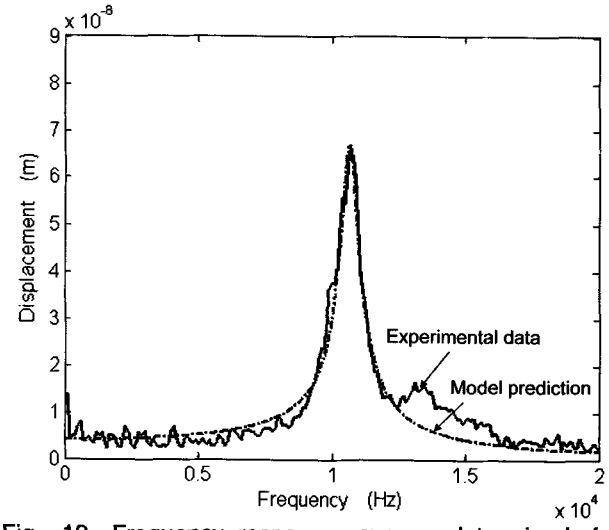

Fig. 13—Frequency–response curves determined from model predictions and experimental data for the diaphragm structure

the in-plane tension, increasing the diaphragm thickness, or decreasing the diaphragm radius. However, trade-offs between bandwidth and sensitivity have to be examined, since a high bandwidth may not mean high sensitivity and vice versa. As pointed out, it is possible to realize high sensitivity and high bandwidth by reducing the diaphragm thickness and applying an appropriate tension. In addition, the inclusion of damping can help extend the flat region of the diaphragm frequency–response curve, resulting in an increased sensor bandwidth. It should be noted that the scope of this paper has been limited to linear behavior, and for larger amplitudes of the loading, nonlinear behavior is possible as pointed out in related work of the first author.[5]

Acknowledgments

The authors gratefully acknowledge partial support received for this work from the U.S. Army Research Office (ARO) under contract No. DAAH 049610334 and from the National Science Foundation through Award No. CMS-0123222. Professor Ed Magrab is thanked for his comments on an earlier version of this paper.

References

1. Matsuoka, Y., Yamamoto, Y., Tanabe, M., Shimada, S., Yamada, K., Yasukawa, A., and Matsuzaka, H., "Low-pressure Measurement Limits for Silicon Piezoresistive Circular Diaphragm Sensors," Journal of Micromechanics and Microengineering, **5**, *32–35 (1995).*

2. Pedersen, M., Meijerink, M.G.H., Olthuis, W., and Bergveld, P., "A Capacitive Differential Pressure Sensor with Polyimide Diaphragm," Journal of Micromechanics and Microengineering, **7**, *250–252 (1997).*

3. Xiao, Z., Engström, O., and Vidovic, N., "Diaphragm Deflection of Silicon Interferometer Structures Used as Pressure Sensors," Sensors and Actuators A, **58**, *99–107 (1997).*

4. Zeng, N., Shi, C., Wang, D., Zhang, M., and Liao, Y., "Diaphragm-type Fiber-optic Interferometric Acoustic Sensor," Optical Engineering, **42** *(9), 2558–2562 (2003).*

5. Yu, M., "Fiber-optic Sensor Systems for Acoustic Measurements," Ph.D. Dissertation, University of Maryland, College Park, MD (2002).

6. Yu, M. and Balachandran, B., "Acoustic Measurements Using a Fiber-optic Sensor System," Journal of Intelligent Material Systems and Structures, **14** *(7), 409–414 (2003).*

7. Zuckerwar, A.J., "Theoretical Response of Condenser Microphone," Journal of the Acoustical Society of America, **64**, *1278–1285 (1978).*

8. Sheplak, M. and Dugundji, J., "Large Deflections of Clamped Circular Plates under Initial Tension and Transitions to Membrane Behavior," ASME Journal of Applied Mechanics, **65** *(1), 107–115 (1998).*

9. Soedel, W., Vibrations of Shells and Plates, Marcel Dekker, New York (1993).

10. Mansfield, E.H., The Bending and Stretching of Plates, Pergamon Press, New York (1964).